

The mafic rocks along the North Tabriz Fault, possible remnants of Neo-Tethys oceanic crust in NW Iran

Fatemeh Mesbahi^{*1,2}, Mohammad Mohajjel¹, Roland Oberhänsli³, Mohsen Moazzen²

¹ Department of geology, Tarbiat Modares University, Tehran, Islamic Republic of Iran.

² Department of Earth Sciences, Faculty of Natural Sciences, University of Tabriz, Tabriz, Islamic Republic of Iran.

³ Institute of Earth and Environmental Science, University of Potsdam, Potsdam Germany.

*Corresponding author, e-mail: mesbahif@tabrizu.ac.ir

(received: 13/05/2017 ; accepted: 29/08/2017)

Abstract

The North Tabriz Fault is seismologically an active fault with current right lateral strike-slip movements. Restricted mafic to intermediate Late Cretaceous igneous rocks are exposed along the North Tabriz Fault. Whole rock and clinopyroxene phenocrysts geochemistry were studied in order to characterize the petrogenesis of these mafic rocks and their possible relation to an oceanic crust. The results indicate a tholeiitic parental magma that formed in an evolved mid-ocean ridge tectonic setting similar to the Iceland mid-Atlantic ridge basalts. The ocean floor basalt characteristics give evidence of an oceanic crust along the North Tabriz Fault. Therefore, the trend of the North Tabriz Fault more likely marks a suture zone related to the closure of a branch of the Neo-Tethys Ocean in the NW Iran. This fault, in addition to the Caucasus and Zagros suture zones, compensates an important part of the convergence between the Arabian and Eurasian plates resulting from the Red Sea divergence. It is concluded that the North Tabriz Fault appears to be possible southeastern continuation of the North Anatolian suture zone.

Keywords: North Tabriz Fault, Mafic Rocks, Tholeiite, Late Cretaceous.

Introduction

The NW-SE trending North Tabriz Fault (NTF) as one of the major geological structures in northwestern Iran is situated between the Caucasus suture to the north and the Zagros suture to the South (Fig. 1). The NTF is a seismologically active fault with recent right lateral strike-slip movements (Berberian, 1976, 1997; Hessami *et al.*, 2003; Karakhanian *et al.*, 2004). Together with the Caucasus and Zagros suture zones the NTF compensates an important part of the compression derived from the convergence between Eurasian and Arabian plates. The NTF also appears to be the southeastern continuation of the North Anatolian Fault and other right-lateral strike-slip faults in SE Turkey (Fig. 1) (Jackson, 1992; Westaway, 1994; Copley & Jackson, 2006).

The NTF is regarded as a collisional suture zone resulting from the closure of the northward subducting Neo-Tethyan back-arc basin in early Cenozoic (Alavi, 1991, 2007; Azizi & Jahangiri, 2007). Considering the Khoy ophiolite (NW Iran, e.g. Hassanipak & Ghazi, 2000; Ghazi *et al.*, 2003; Moazzen & Oberhänsli, 2008) and some of the mafic and ultramafic bodies along the NTF (e.g. Misho, Moro, Vaniar and Eskandar) Azizi & Jahangiri (2007) postulated a narrow oceanic basin (the Khoy-Zanjan oceanic basin) that was subducted beneath the Alborz-Azerbaijan plate in

the Eocene. This should have led to the formation of the Alborz-Azerbaijan volcanic belt north of the NTF at the southern rim of the Alborz-Azerbaijan plate.

Sparse and limited remnants of basic rocks, presumably Late Cretaceous oceanic crust occur along the NTF (Ahankoub & Jahangiri, 2013; Asadian, 1993). The Late Cretaceous basic rocks are exposed in the Moro and Misho mountains, Vaniar complex (study area) and Eskandar assemblage (Fig. 2). The Moro and Misho mountains are comprised of a wide range of sedimentary, volcanic and intrusive rocks with Paleozoic to Mesozoic ages (Asadian, 1993; Asadian *et al.*, 1994; Saccani *et al.*, 2013; Ahankoub & Jahangiri, 2013). The Vaniar Late Cretaceous rocks, north of Tabriz, on the northern side of the NTF and the Late Cretaceous Eskandar assemblage (Fig. 2) are composed of pelagic limestone, silty sandstone, chert layers and basaltic rocks (Faridi *et al.*, 2006). While other Late Cretaceous volcanic exposures along the NTF are strongly altered, the Vaniar mafic rocks are relatively fresh and easily accessible. These mafic rocks are key exposures of the Late Cretaceous volcanic rocks to decipher their origin and relation to a suture as well as the tectonic setting of the NTF. The petrological and geochemical characteristics of the Vaniar mafic rocks were not studied previously.

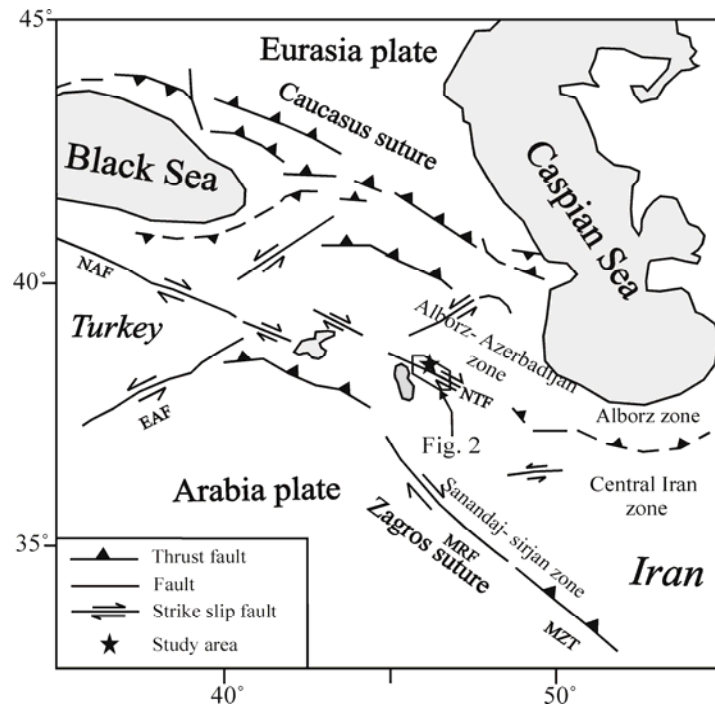


Figure 1. Geological map of the NW Iran and adjacent areas. The study area on the northern block of the North Tabriz Fault (NTF) is located between the Caucasus suture to the north and the Zagros suture to the south (modified after Jackson, 1992). NAF: North Anatolian Fault, EAF: East Anatolian Fault, MRF: Main Recent Fault, MZT: Main Zagros Thrust.

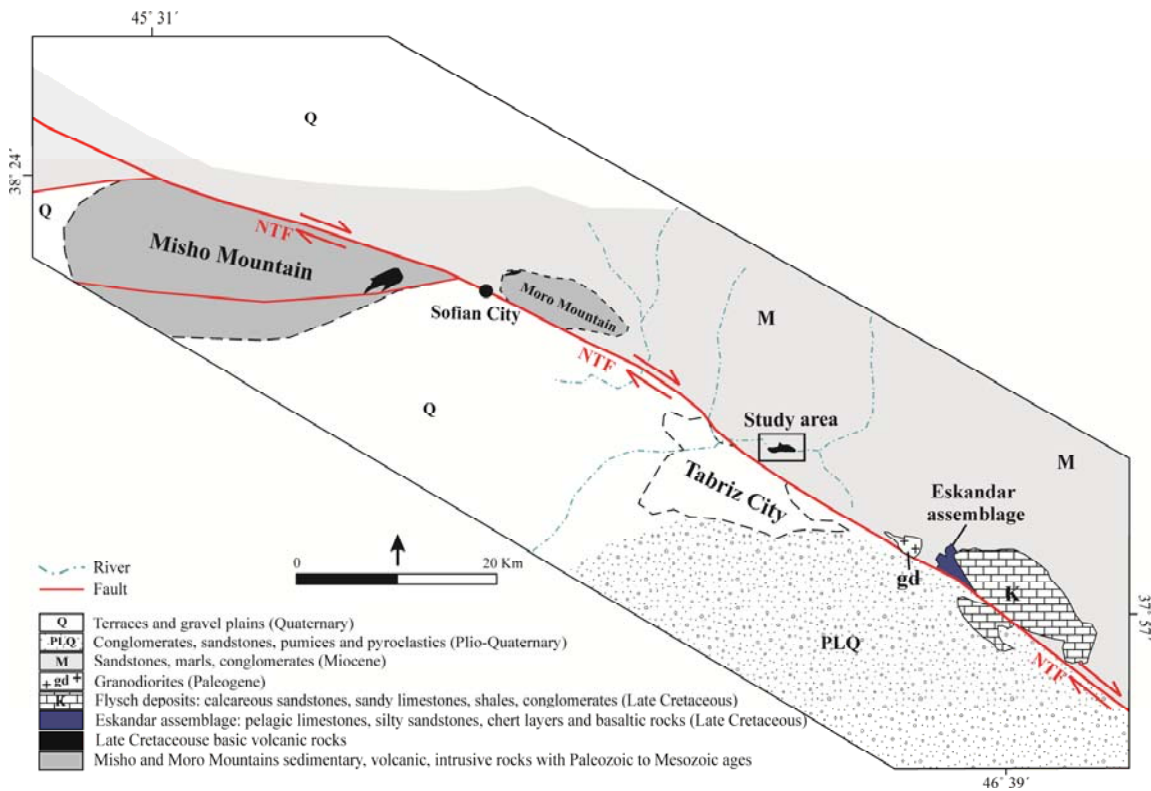


Figure 2. Simplified geological map of the study area and adjacent areas.

This contribution adds data on petrology and geochemistry of the Vaniar mafic rocks and tries to reveal their tectonic setting.

Materials and methods

For studying the petrography, geochemistry and tectonic setting of the Vaniar volcanic rocks, more than 40 samples were collected, following detailed field geology studies. Thin sections were prepared to study the petrography. 16 samples from the weakly altered rocks were selected for whole rock analysis. They were analyzed by XRF and ICP-MS for the major oxides and trace elements (Table 1). The analyses were carried out at the University of Potsdam and the Geo-Forschung-Zentrum in Potsdam, Germany. Sample locations are given in Figure 3. Five optically well characterized samples with adequate and fresh phenocrysts of clinopyroxene were selected for electron microprobe analysis (Table 2) with a JEOL JXA-8800 microprobe at Potsdam University. An accelerating voltage of 15 kV, specimen current of 20 nA and beam diameters of 1-3 μ m were used. Counting time was 30 seconds on peaks and 15 on background. Natural and synthetic standards (Fe₂O₃ (Fe), rhodonite (Mn), rutile (Ti), MgO (Mg), wollastonite (Si, Ca), fluorite (F), orthoclase (Al, K) and albite (Na)) were used for calibration.

Geology and petrography

The studied mafic volcanic rocks are exposed in a small area in the deep valley of the Ajichay River (Fig. 3). The mafic rocks are non-conformably covered by detrital, sub-horizontal Miocene red beds (Fig. 4a). Based on petrology and stratigraphy, Faridi & Khodabandeh (2011) correlated the Vaniar volcanic rocks with the Late Cretaceous mafic rocks of the Eskandar assemblage. The volcanic (basalt, andesitic basalt) and sedimentary (pelagic limestone, silty sandstone, chert layers, pyroclastics) rocks of the Eskandar assemblage are strongly cataclastic and bounded by faults (Faridi *et al.*, 2006; Faridi & Khodabandeh, 2011). Basalts and andesitic basalts of the Eskandar assemblage show amygdales filled by calcite, epidote and silica. Plagioclase is completely altered to clay minerals. The glassy groundmass is hydrated and chloritized.

From pelagic limestones in the Eskandar area Faridi *et al.* (2006) reported Late Cretaceous microfossils (*Globotruncana magarensis*, *Globotruncana lapparanti*, *Globotruncana sp.*, *Hedbergella sp.*, radiolaria and spicules).

Since the basic rocks intercalate with the Late Cretaceous pelagic limestones, the stratigraphic age of the basic rocks is considered to be Late Cretaceous (Faridi *et al.*, 2006).

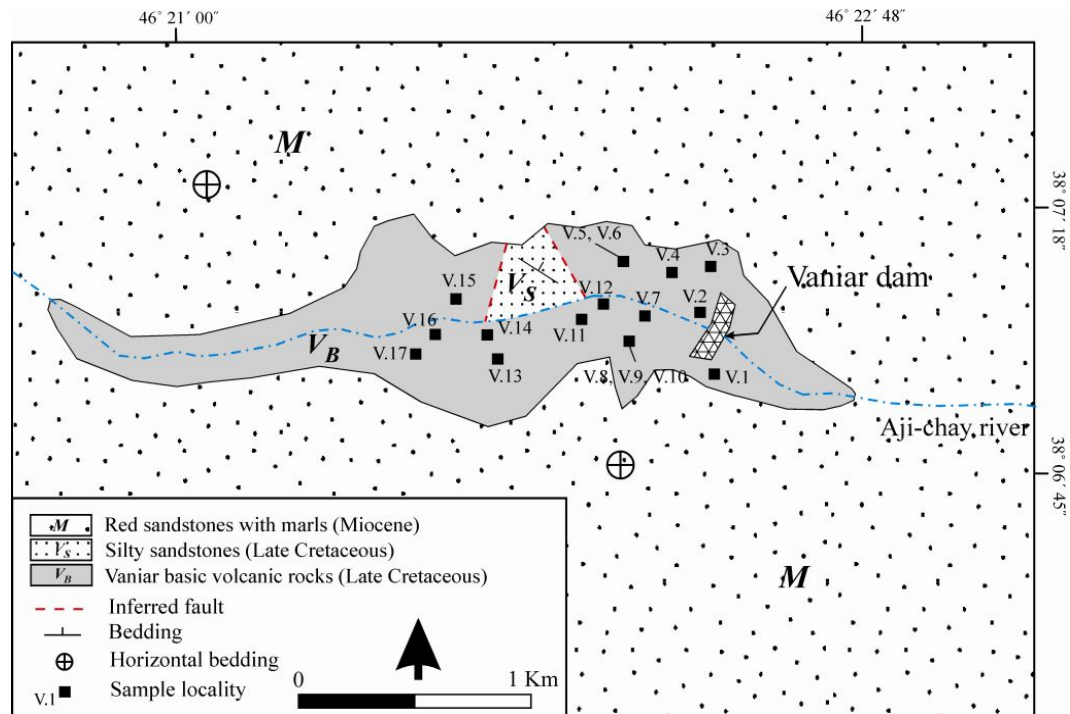


Figure 3. Simplified geological map of the Vaniar area and sample localities.

Table 1. Whole rock composition of the studied samples.

Sample	V.2	V.3	V.4	V.5	V.6	V.7	V.8	V.9	V.10	*V.11	*V.12	V.13	V.14	*V.15	*V.16	*V.17
Major oxides, wt%																
SiO ₂	48.50	50.80	49.70	52.30	48.70	49.50	52.60	51.70	59.80	49.30	49.10	44.40	51.60	48.90	41.80	48.20
TiO ₂	1.48	1.51	1.49	1.40	1.40	1.63	1.06	0.96	0.81	1.64	1.23	1.12	0.87	1.12	1.59	1.22
Al ₂ O ₃	18.80	16.60	16.30	17.50	18.70	17.60	16.30	14.70	13.30	17.20	17.30	17.80	17.10	16.00	17.90	17.40
Fe ₂ O ₃	9.68	8.39	8.27	8.02	8.90	9.44	6.21	9.73	7.43	9.58	10.94	11.75	7.92	10.41	13.05	10.79
MnO	0.16	0.13	0.19	0.12	0.15	0.16	0.09	0.10	0.07	0.18	0.17	0.13	0.08	0.11	0.13	0.19
MgO	5.21	4.88	4.68	4.87	5.26	5.12	3.18	6.81	5.37	5.71	4.61	8.61	5.36	7.35	8.67	5.14
CaO	4.19	6.23	9.42	3.50	5.28	6.40	9.78	6.71	4.99	4.67	10.20	5.15	5.81	5.23	6.43	10.27
Na ₂ O	5.15	5.56	3.00	6.54	5.11	3.71	3.48	2.83	2.82	5.31	2.38	3.24	5.57	4.70	2.17	2.32
K ₂ O	0.86	0.27	0.84	0.28	0.50	0.77	0.73	0.20	0.16	0.59	0.60	0.66	0.21	0.21	1.05	0.65
P ₂ O ₅	0.22	0.20	0.26	0.28	0.32	0.22	0.20	0.08	0.34	0.28	0.19	0.15	0.21	0.17	0.14	0.19
LOI	5.19	5.27	5.60	5.01	5.27	5.21	5.79	5.52	4.54	5.21	2.93	6.71	4.93	5.60	6.72	3.40
Total	99.45	99.85	99.75	99.81	99.58	99.76	99.43	99.33	99.63	99.66	99.65	99.72	99.67	99.80	99.65	99.76
Trace elements, ppm																
Ba	280	160	312	163	270	276	161	132	153	284	225	275	157	197	337	213
Ce	22.2	22.5	24.5	22.2	28.2	24.7	26.8	16.1	30.4	24.5	21.6	22.2	24.3	20.9	36.7	19
Cr	39	57	56	43	44	55	59	72	47	53	47	69	72	77	113	48
Dy	3.01	3.82	3.93	4.29	4.3	3.98	3.21	2.24	4.45	4.25	3.45	3.52	3.08	3.22	5.25	2.66
Er	1.75	2.24	2.25	2.49	2.41	2.27	1.84	1.33	2.66	2.39	2.01	2	1.94	1.9	3.11	1.57
Eu	1.64	4.13	2.08	2.84	2.38	2.07	1.65	1.88	1.84	4.79	2.74	3.78	3.61	3.8	4.45	1.76
Ga	15	20	17	15	18	17	14	15	12	17	16	17	14	12	17	17
Gd	3.73	5.72	4.5	5.05	5.17	4.49	3.73	2.96	4.92	6.49	4.46	5.36	4.84	5.12	7.01	3.4
Ho	<0.5	<0.5	<0.5	<0.5	<0.5	<0.5	<0.5	<0.5	<0.5	<0.5	<0.5	<0.5	<0.5	<0.5	<0.5	<0.5
K	7139	2241	6973	2324	4151	6392	6060	1660	1328	4898	4981	5479	1743	1743	8717	5396
La	11.5	9.6	10.6	9.6	12.3	9.9	12.8	7.2	14.6	10.3	9.9	8.9	11.6	8.9	16.9	9.3
Lu	<0.5	0.58	<0.5	<0.5	<0.5	<0.5	<0.5	<0.5	<0.5	0.64	<0.5	0.53	0.52	0.55	0.7	<0.5
Nb	9	12	10	12	9	12	9	9	9	10	9	10	9	9	12	9
Nd	16	28.2	18.7	22.9	20.9	18.1	16.8	12	18.6	30.1	21.2	24.9	21	22.4	30.1	13.8
Ni	23	31	26	20	23	33	16	28	22	27	15	28	28	28	40	18
Pr	2.48	1.4	2.1	2.31	3.04	2.68	2.14	1.21	3.16	2.27	<0.5	1.37	1.29	1.48	3.68	1.34
Rb	33	22	27	21	24	27	24	21	19	26	23	27	22	18	37	23
Sc	18.3	22.3	21.5	18.7	21.2	23	18.2	23	14.2	21.5	23.9	21.9	19	25.6	38	19.2
Sm	2.9	3.55	3.56	3.65	4.13	3.62	3.19	2.12	3.93	4.21	3.14	3.62	2.9	3.13	4.89	2.58
Sr	603	287	371	213	659	338	390	269	215	462	479	326	217	345	295	491
Tb	0.86	2.15	1.24	1.5	1.18	1.11	0.93	0.88	1	2.17	1.66	1.78	1.63	1.7	2.04	0.98
Ti	8897	9076	8933	8369	8381	9790	6361	5725	4856	9814	7344	6738	5240	6690	9538	7314
Tm	1.83	6.34	2.25	4.3	2.2	1.98	1.39	1.5	1.31	6.74	3.94	5.13	3.56	4.47	4.62	1.67
V	238	255	235	259	233	264	218	217	144	273	245	186	191	172	243	255
Y	21	19	21	22	24	22	17	11	26	22	17	16	15	16	25	18
Yb	1.52	1.87	1.92	1.9	2	1.88	1.54	1.31	2.32	1.99	1.76	1.68	1.7	1.74	2.77	1.41
Zn	100	117	121	135	115	148	265	135	140	135	116	97	124	100	106	113
Zr	102	84	86	77	97	90	95	79	70	94	84	98	78	98	134	85

* Samples in which clinopyroxene is analyzed by microprobe (Table 2).

The Eskandar assemblage has been intruded by Paleocene granodiorites and is overlain by Miocene sedimentary beds (Faridi *et al.*, 2006). In the Vaniar area, a layered silty sandstone unit (Fig. 4b and c) comparable with silty sandstone beds in the Eskandar assemblage is exposed along with the mafic volcanic rocks. Both the layered silty sandstone and mafic volcanic rocks are unconformably covered by Miocene red beds. The volcanic rocks experienced intense brittle deformation (Faridi & Khodabandeh, 2011).

The Vaniar mafic rocks show a simple petrographic composition. They are generally

basaltic with porphyritic texture containing phenocrysts of clinopyroxene and plagioclase embedded in a matrix with very fine (in micron scale) plagioclase, volcanic glass and secondary minerals such as chlorite (Fig. 5a). Amygdules are filled by secondary silica and calcite (Fig. 5b). The size of plagioclase phenocrysts is up to several millimeters. They are euhedral to subhedral and are partially altered to secondary minerals (Fig. 5a). Clinopyroxene phenocrysts are euhedral to subhedral (Fig. 5a and c) and up to 2 millimeters in size. They are mostly fresh but where fractured they show alteration along the fractures.

Table 2. Representative microprobe analyses of clinopyroxene phenocrysts in the Vaniar basaltic rocks.

sample	V.1	*V.11	*V.12	*V.15	*V.16	*V.17
SiO ₂	50.08	50.28	50.52	49.94	50.61	50.56
TiO ₂	0.70	0.84	0.64	0.80	0.68	0.78
Al ₂ O ₃	4.72	3.97	3.72	4.24	3.80	3.59
FeO	7.75	7.88	8.81	9.79	8.42	9.24
MnO	0.15	0.18	0.23	0.24	0.20	0.23
MgO	15.12	15.34	15.70	14.65	15.31	14.84
CaO	21.13	20.79	20.00	20.02	20.63	20.48
Na ₂ O	0.30	0.29	0.28	0.30	0.28	0.30
K ₂ O	0.00	0.00	0.00	0.00	0.00	0.00
Cr ₂ O ₃	0.17	0.08	0.15	0.03	0.12	0.04
Total	100.13	99.67	100.04	100.01	100.06	100.06
Formula based on 6(O) and 4 cations						
Si	1.843	1.860	1.864	1.853	1.868	1.873
Ti	0.019	0.023	0.018	0.022	0.019	0.022
Al	0.205	0.173	0.162	0.185	0.165	0.157
Fe	0.239	0.244	0.272	0.304	0.260	0.287
Mn	0.005	0.006	0.007	0.008	0.006	0.007
Mg	0.829	0.846	0.863	0.810	0.842	0.819
Ca	0.833	0.824	0.790	0.795	0.816	0.813
Na	0.021	0.021	0.020	0.022	0.020	0.021
Cr	0.005	0.002	0.004	0.001	0.004	0.001
Total	4.000	4.000	4.000	4.000	4.000	4.000
Wo	46.51	45.54	43.65	44.25	44.89	44.62
En	46.27	46.74	47.62	44.97	46.33	44.96
Fs	7.22	7.72	8.74	10.78	8.78	10.42

* Samples that have been analyzed by whole rock analysis (Table 1).

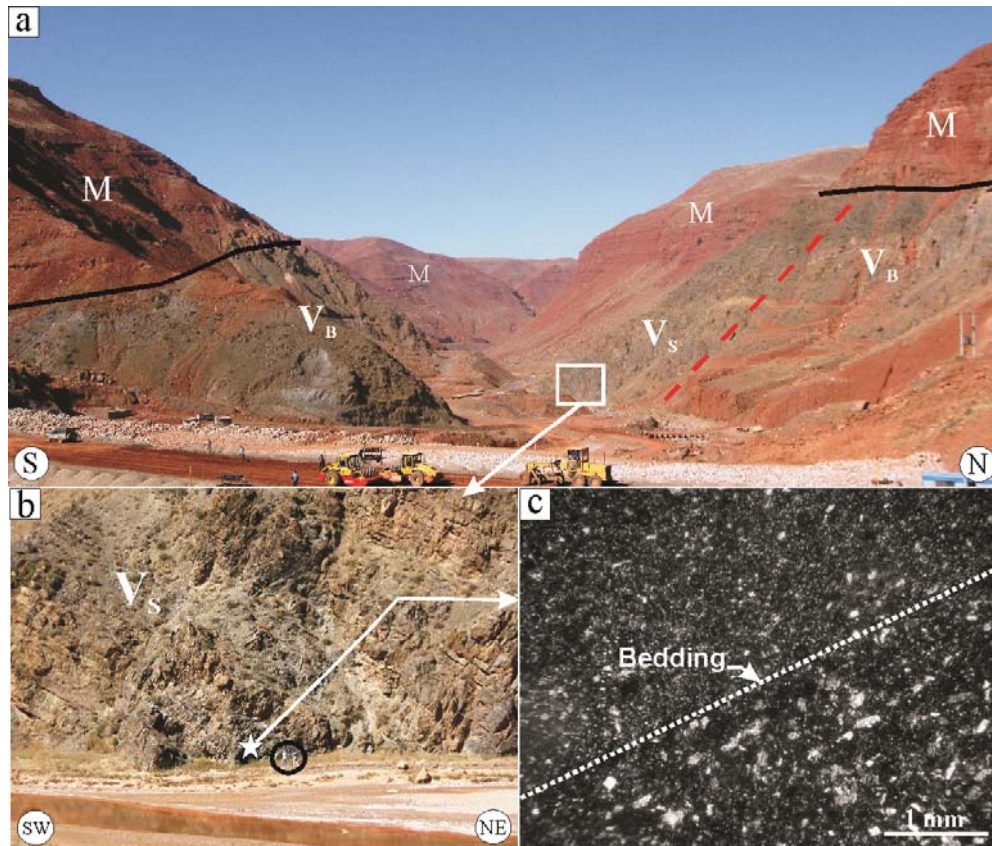


Figure 4. a: The Vaniar basic rocks (V_B) and silty-sandstone layers (V_S) is overlain by Miocene red beds (M), at the Vaniar dam construction site. b: The exposure of silty-sandstone layers (V_S). c: Thin section of silty-sandstone with bedding trace.

Some of the clinopyroxene phenocrysts show weak optical zoning (Fig. 5d).

Whole rock geochemistry

Analyses of major oxides and trace elements of 16 optically well-characterized, representative samples from the mafic rocks with minimal alteration are given in Table 1. Since the volcanic rocks of the study area are partially altered, we used the immobile elements in order to study the geochemistry and tectonic setting of these rocks. Generally the rare earth elements (REE), Sc, Y, Th, Zr, Hf, Ti, Nb, Ta, and P are considered to be immobile (Pearce, 1983). Co, Ni, V and Cr can be considered as immobile elements during alteration (Rollinson, 1993). Based on Zr/TiO₂ versus Nb/Y ratios of Winchester & Floyd (1977) almost all the samples plot in the field of sub-alkaline basalts (Fig. 6a). The Nb/Y versus Zr/P₂O₅ diagram (Floyd & Winchester, 1975) provides the best discrimination between alkali and tholeiitic basalts (Rollinson, 1993). In this diagram the samples plot into the field of tholeiitic basalts (Fig. 6b). In a Ti

versus V diagram (Shervais, 1982) (Fig. 7a) the studied rocks plot as ocean floor basalts (OFB) including both mid ocean ridge basalts (MORB) and back arc basin basalts (BAB).

Pearce & Cann (1973) designed Ti-Zr and Ti-Zr-Y discrimination diagrams for tholeiitic basalts with 20 % <CaO+MgO>12%. For altered rocks with CaO+MgO < 12% other discrimination diagrams should be applied to verify if the rocks were originally basalts (Prestvik, 1982). The Vaniar volcanic rocks are altered and their CaO+MgO content is less than 12%, however based on Zr/TiO₂ versus Nb/Y (Fig. 6a) and Nb/Y versus Zr/P₂O₅ diagrams (Fig. 6b) the Vaniar basic rocks are tholeiitic basalts. Therefore, Ti-Zr and Ti-Zr-Y discrimination diagrams of Pearce & Cann (1973) can be applied. Most of the samples plot in the within plate basalts field in the Ti-Zr-T triangular diagram (domain D in Fig. 7b). A few samples plot into domain B that includes ocean floor basalts, ocean island tholeiites and calc-alkaline basalts (Fig. 7b).

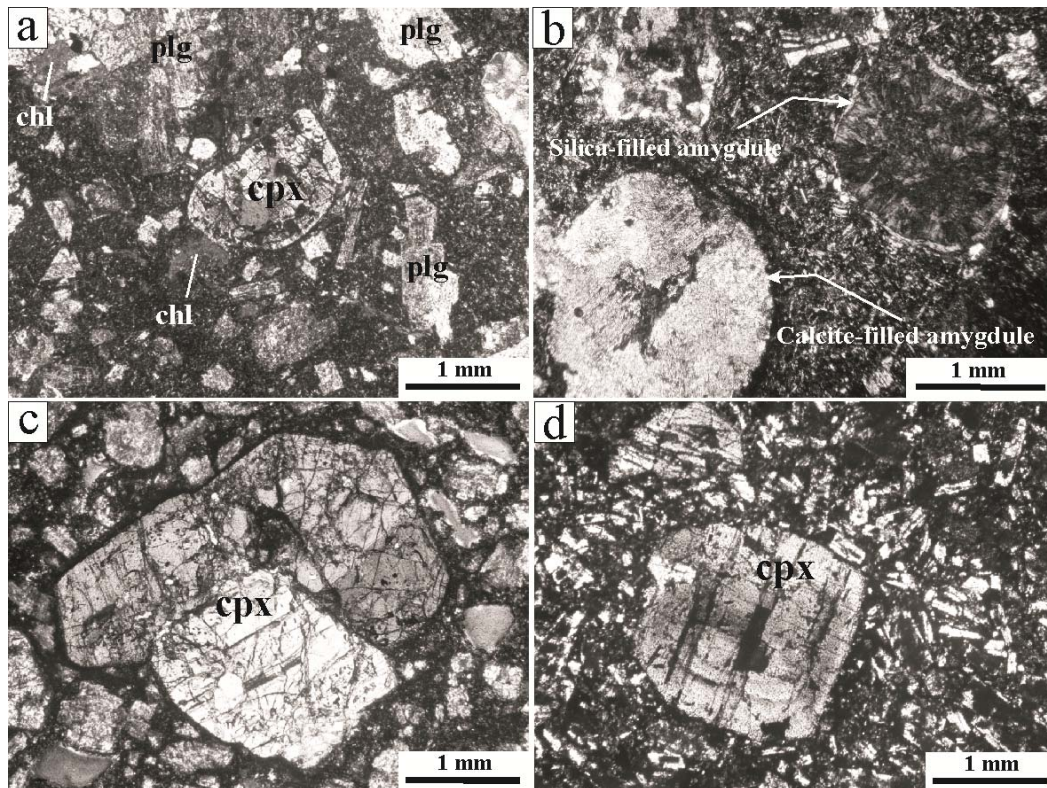


Figure 5. Petrographic features of the Vaniar basic rocks. a: Plagioclase (plg) and clinopyroxene (cpx) phenocrysts and chlorite (chl) as a secondary mineral in a fine grained matrix. The middle part of subhedral clinopyroxene is altered. b: Silica and calcite filled amygdules. c: Intergrowth texture of euhedral phenocrysts of clinopyroxenes. d: Weak optical zoning in clinopyroxene phenocryst. (All photos crossed polarized light).

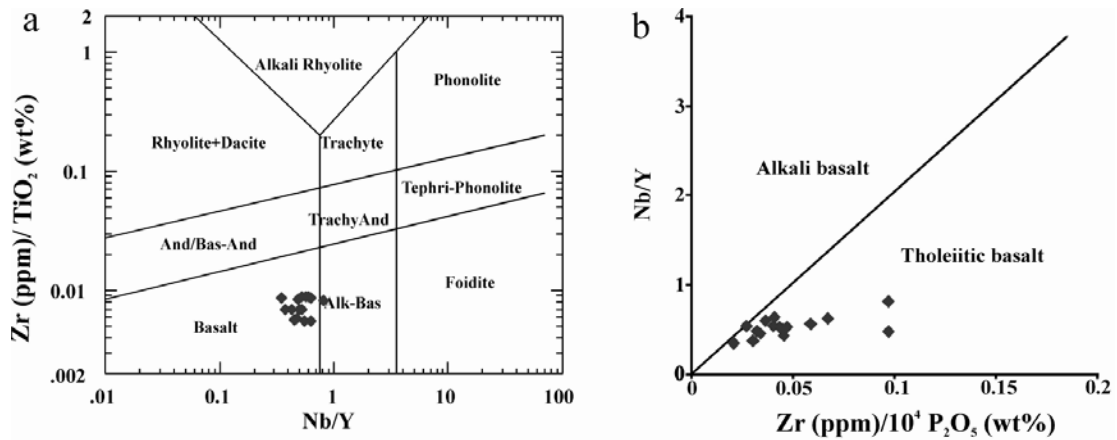


Figure 6. a: Zr/ TiO₂ vs Nb/Y diagram (Winchester & Floyd, 1977) shows that almost all samples are plotted in the basalt field. b: In the Nb/Y-Zr/P₂O₅ (Floyd & Winchester, 1975) all samples show tholeiitic characteristics.

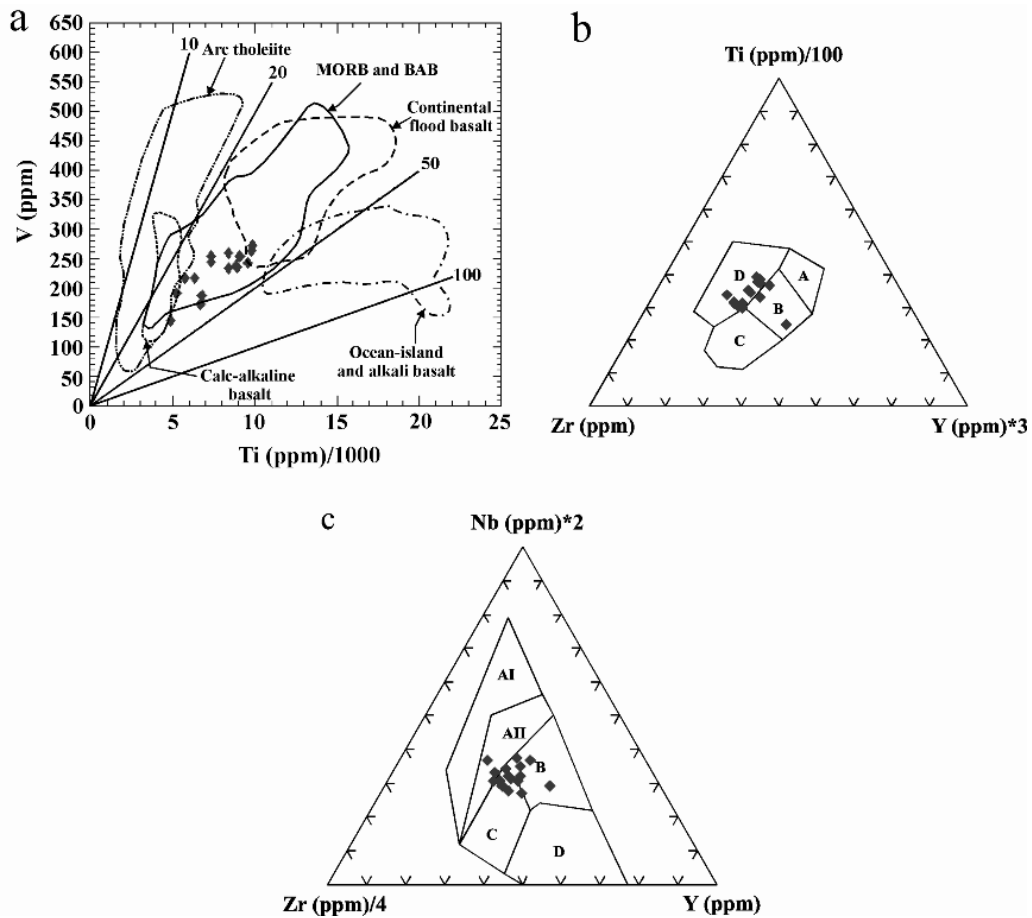


Figure 7. a: In the Ti vs V diagram (Shervais, 1982) the samples show MORB or back arc basin basalt (BAB) characteristics; b: in a Ti-Zr-Y plot (Pearce & Cann, 1973) most samples project as within plate basalts (D). (B: MORB, island arc tholeiites and calc-alkaline basalts, C: calc-alkaline basalts, A: island arc tholeiites); c: Nb-Zr-Y diagram (Meschede, 1986) indicates E- type MORB (field B), (C: within plate tholeiites and island arc basalts, AII: alkaline and tholeiitic within plate basalts. D: N- type MORB, AI: alkaline within plate basalts).

In the Nb-Zr-Y diagram (Meschede, 1986) some samples plot in the field of within plate tholeiites (domains AII and C in Fig. 7c), some plot in the

field for evolved mid-ocean ridge basalts (E-MORB, domain B in Fig. 7c).

In spider diagrams normalized to C1 chondrites

(Sun & McDonough, 1989) and mid ocean ridge basalt (Bevins *et al.*, 1984) the Vaniar mafic rocks are compared to normal MORB (N-MORB), evolved MORB (E-MORB), alkaline within plate basalts (WPA), calc-alkaline basalt (CAB) and island arc tholeiites (IAT) (Fig. 8a, b). In REE diagram normalized to C1 chondrites the Vaniar samples are compared to normal MORB (N-MORB) and evolved MORB (E-MORB). The data sources for other basalts are from Sun (1980).

In all spider diagrams, the Vaniar trace element patterns are similar to E-MORB (Fig. 8a, b) but show enrichment in K, Ba and Rb that could be due to the extremely enriched mantle source like a plum below the MORB that is similar to Iceland. In the REE diagram the Vaniar REE elements patterns is more coincident with E-MORB.

Mineral chemistry of clinopyroxene phenocrysts

The composition of clinopyroxene phenocrysts reflects the chemical differences between different basaltic magma types more precisely than whole rock compositions in altered rocks (Vallance, 1974; Mevel & Velde, 1976; Nisbet & Pearce, 1977). Therefore, the chemistry of clinopyroxene phenocrysts can be used as discrimination for basalts from different tectonic settings (Rollinson, 1993). 45 unaltered clinopyroxene phenocrysts from 6 individual mildly altered rock samples were selected for microprobe analysis. A total of 500 points were analyzed. Since the composition of clinopyroxenes is almost identical in different parts of the crystals, representative compositions of individual crystals and atomic proportions are reported in Table 2. In the Wo-En-Fs diagram of Morimoto *et al.* (1988) the studied clinopyroxenes plot in the diopside and augite fields (Fig. 9a).

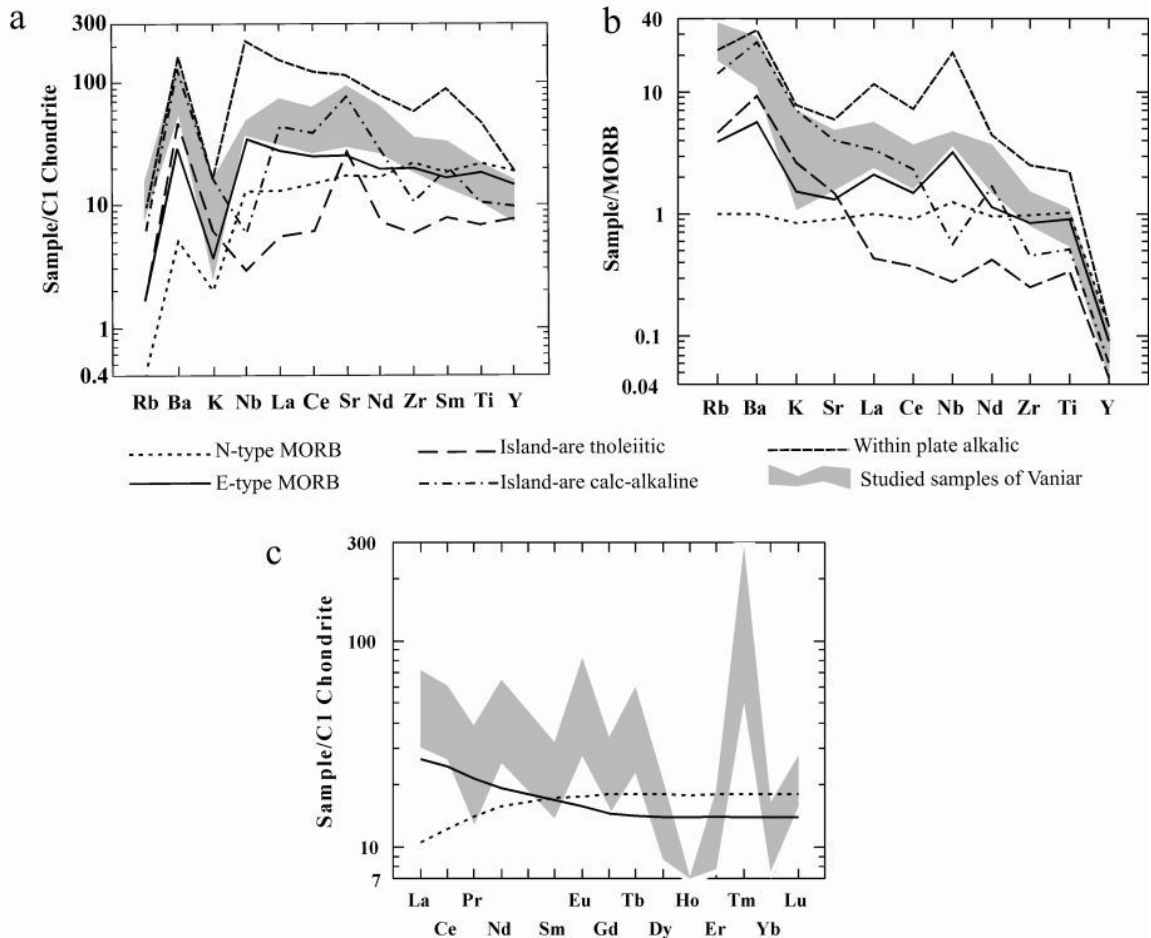


Figure 8. Spider and REE diagrams for Vaniar samples and basalts from different tectonic settings. Data sources for other basalts from Sun (1980). a: C1 chondrite normalized spider diagram. Normalization values from Sun & McDonough (1989). b: MORB normalized spider diagram. Normalization values from Bevins *et al.* (1984). c: C1 chondrite normalized REE diagram. Normalization values from Sun & McDonough (1989).

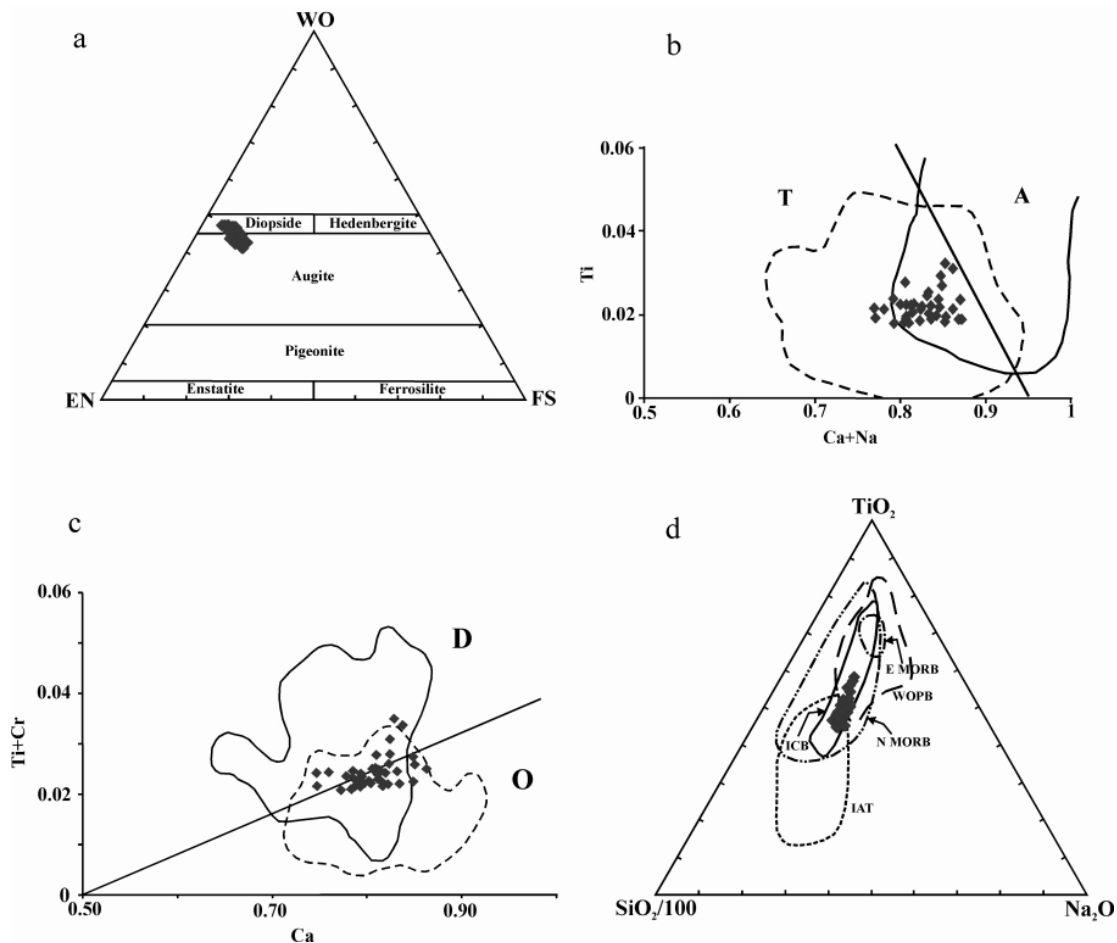


Figure 9. Classification diagrams for clinopyroxene. a: in a WO-EN-FS diagram (Morimoto *et al.*, 1988) all samples plot as diopside and augite. b: Using Ti vs Ca+Na (Leterrier *et al.*, 1982) they have sub-alkaline characteristics. (A: alkaline, T: sub-alkaline). c: In the Ti+Cr vs Ca diagram (Leterrier *et al.*, 1982) the samples have a tendency to orogenic (Island arc) field. (D: non-orogenic, O: orogenic). (d) In a TiO_2 - SiO_2 - Na_2O diagram (Beccaluva *et al.*, 1989) the analyses plot in the field of Icelandic basalts (ICB). (WOPB: within ocean floor basalts, IAT: island arc tholeiites)

To discriminate between alkali basalts, spreading center tholeiites and island-arc basalts, Na, Al, Ca, Cr, and Ti contents of clinopyroxene can be used (Leterrier *et al.*, 1982). In the Ti versus Ca+Na diagram, all samples plot in the field of sub-alkaline basalts (domain T in Fig. 9b). Using Ti+Cr versus Ca, in light of the distribution of data in both orogenic and non-orogenic domains, a weak orogenic tendency seems obvious (Fig. 9c). In the TiO_2 - SiO_2 - Na_2O diagram of Beccaluva *et al.* (1989), all samples plot in the field of Icelandic basalt (ICB in Fig. 9d).

Discussion and conclusion

Based on the whole rock analysis, the Vaniar mafic rocks resemble tholeiitic basalts (Fig. 6a, b).

Considering the immobility of Ti and V in a wide range of temperature and water / rock ratios, these

elements can be applied to classify altered basic rocks (Shervais, 1982). In the Ti-V discrimination diagram the Vaniar samples relate to ocean floor basalts, including both MORB-type and back arc basin basalts (Fig. 7a). Few indications point to a within plate tholeiite origin (Fig. 7b; domains AII and C in Fig. 7c) but the majority of samples represent evolved MORB as supported by the trace element distribution in spider and REE diagrams (Fig. 8). Prestvik (1982) showed that when rocks are altered or when a mid-ocean ridge is evolved, as for example in Iceland (basalts enriched in Fe, Ti and LREE), samples plot in the field of within plate basalts due to anomalous mantle compositions rather than tectonic setting.

In conclusion, discrimination and spider diagrams imply that the Vaniar basalts formed as extremely evolved mid-ocean-ridge basalt (E-

MORB) and deviation towards within plate basalts in the Ti-Zr-Y diagram can be attributed to the evolved nature of these rocks, similar to Icelandic basalts. The chemistry of clinopyroxene phenocrysts implies that the Vaniar volcanic rocks are sub-alkaline basalts with weak orogenic (Island arc) tendency (Fig. 9b). Whereas in the TiO₂-SiO₂-Na₂O diagram of Beccaluva *et al.* (1989) the analyzed pyroxenes are clearly of Icelandic basalts type (Fig. 9d).

Based on both whole rock and clinopyroxene chemistry, the original Vaniar basalt magma formed at an evolved mid-ocean-ridge similar to the anomalous Iceland mid-Atlantic ridge. The oceanic

crust affinity of the Late Cretaceous Vaniar basalts corroborates the proposed Late Cretaceous oceanic crust (Alavi, 1991, 2007; Azizi & Jahangiri, 2007) along the NTF and thus a Paleogene suture zone between the Caucasus and Zagros suture zones.

Acknowledgments

This research was supported financially by Tarbiat Modares University through a grant to Ph.D. thesis of the first author. We thank Antje Musiol and Christina Gunter for their help with the analyses. We are grateful to Prof. Noori-Dalooi for his helps.

References

- Alavi, M., 1991. Tectonic map of Middle East. Geological survey of Iran, scale 1: 2900,000.
- Alavi, M., 2007. Structure of the Zagros fold-thrust belt in Iran. *American Journal of Sciences*, 307: 1064-1095.
- Ahankoub, M., Jahangiri, A., 2013. Lower-crust source for the Misho A-type granites from North West Tabriz, Iran: Geochemistry and Nd-Sr isotopic evidence. 2nd International Conference on Earth Science and Climate Change, Embassy Suites Las Vegas, NV, USA.
- Asadian, A., 1993. Geology map of Tabriz, Iran. Geological Survey of Iran, scale 1:100,000.
- Asadian, A., Mirzaee, A.R., Mohajjel, M., Hadjililou, B., 1994. Geology map of Marand, Iran. Geological Survey of Iran, scale 1:100,000.
- Azizi, H., Jahangiri, A., 2007. Cretaceous subduction-related volcanism in the northern Sanandaj-Sirjan Zone, Iran. *Journal of Geodynamics*, 45: 178-190.
- Beccaluva, L., Macciotta, G., Piccardo, G.B., Zeda, O., 1989. Clinopyroxene composition of ophiolite basalts as petrogenetic indicator. *Chemical Geology*, 77: 165-182.
- Berberian, M., 1976. Contribution to the seismotectonics of Iran, Part II, Geological Survey of Iran. Report 39, 516 pp.
- Berberian, M., 1997. Seismic sources of the Transcaucasian historical earthquakes. In: Giardini, D., Balassanian, S. (Eds), *Historical and Prehistorical Earthquakes in the Caucasus*. Kluwer Academic Publishing, Dordrecht, Netherlands, pp 233-311.
- Bevins, R.E., Kokelaar, B.P., Dunkley, P.N., 1984. Petrology and geochemistry of lower to middle Ordovician igneous rocks in Wales: a volcanic arc to marginal basin transition. *Proceedings of the Geologists' Association*, 95: 337-347.
- Copley, A., Jackson, J., 2006. Active tectonics of the Turkish-Iranian plateau. *Tectonics*, 25:TC6006.
- Faridi, M., Haghfarshi, A., Zamanimehr, S., Sayyedi, P., Allahmadadie, S.H., Khalatbari, M., 2006. Geology map of Khoja, Iran. Geological Survey of Iran. Scale 1: 100,000.
- Faridi, M., Khodabandeh, A., 2011. Explanatory text of the geology map of Tabriz 1 (scale 1: 25,000), Iran. Geological Survey of Iran, 60 pp (in Persian).
- Floyd, P.A., Winchester, J.A., 1975. Magma type and tectonic setting discrimination using immobile elements. *Earth and Planetary Science Letters*, 27: 211-218.
- Ghazi, A.M., Pessagno, E.A., Hassanipak, A.A., Kariminia, S.M., Duncan, R.A., Babaie, H.A., 2003. Biostratigraphic zonation and 40Ar/39Ar ages for the Neotethyan Khoyophiolite of NW Iran. *Palaeogeography, Palaeoclimatology, Palaeoecology*, 193: 311-323.
- Hassanipak, A.A., Ghazi, A.M., 2000. Petrology, geochemistry and tectonic setting of the Khoyophiolite, northwest Iran: implications for Tethyan tectonics. *Journal of Asian Earth Sciences*, 18: 109-121.
- Hessami, K., Pantosti, D., Tabasi, H., Shabanian, E., Abbasi, M.R., Feghhi, K., Soleymani, S., 2003. Paleoearthquakes and slip rates of the North Tabriz Fault, NW Iran: preliminary results. *Annals of geophysics*, 46: 903-915.
- Jackson, J., 1992. Partitioning of strike-slip and convergent motion between Eurasia and Arabia in Eastern Turkey and the Caucasus. *Journal of Geophysical Research*, 97: 12471-12479.
- Karakhanian, A., Jrbashyan, R., Trifonov, V., Philip, H., Avagyan, A., Hessami, K., Jamali, F., Bayraktutan, M., Bagdassarian, H., Arakelian, S., Davtian, V., Adilkhanyan, A., 2004. Active faulting and natural hazards in Armenia, eastern Turkey and Northern Iran. *Tectonophysics*, 380: 189-219.
- Leterrier, J., Maury, R.C., Thonon, P., Girard, D., Marchel, M., 1982. Clinopyroxene composition as a method of identification of the magmatic affinities of paleo-volcanic series. *Earth and Planetary Science Letters*, 59: 139-154.

- Meschede, M., 1986. A method of discriminating between different types of mid-ocean ridge basalts and continental tholeiites with the Nb-Zr-Y diagram. *Chemical Geology*, 56:207-218.
- Mevel, C., Velde, D., 1976. Clinopyroxenes in Mesozoic pillow lavas from the French Alps: influence of cooling rate on compositional trends. *Earth and Planetary Science Letters*, 32: 158-164.
- Moazzen, M., Oberhänsli, R., 2008. Whole rock and relict igneous clinopyroxene geochemistry of ophiolite-related amphibolites from NW Iran – Implications for protolith nature. *Journal of Mineralogy and Geochemistry*, 185(1): 51-62.
- Morimoto, N., Fabries, J., Ferguson, A.K., Ginzburg, I.V., Ross, M., Seifert, F.A., Zussman, J., Aoki, K., Gottardi, G., 1988. Nomenclature of pyroxenes. *Mineralogical Magazine*, 52: 535-550.
- Nisbet, E.G., Pearce, J.A., 1977. Clinopyroxene composition in mafic lavas from different tectonic settings. *Ibid*, 63: 149-160.
- Pearce, J.A., Cann, J.R., 1973. Tectonic setting of basic volcanic rocks determined using trace element analysis. *Earth and Planetary Science Letters*, 19: 290-300.
- Pearce, J.A., 1983. Role of the subcontinental lithosphere in magma genesis at active continental margins. In: Hawkesworth, C.J., Norry, M.J. (Eds), *Continental basalts and mantle xenoliths*. Shiva, Nantwich, pp 230-249.
- Prestvik, T., 1982. Basic volcanic rocks and tectonic setting. A discussion of the Zr-Ti-Y discrimination diagram and its suitability for classification purposes. *Lithos*, 15: 241-247.
- Rollinson, H., 1993. *Using geochemical data: evaluation, presentation, interpretation*: 1st Ed, Longman Group, UK, 352 pp.
- Saccani, E., Azimzadeh, Z., Dilek, Y., Jahangiri, A., 2013. Geochronology and petrology of the Early Carboniferous Misho Mafic Complex (NW Iran), and implications for the melt evolution of Paleo-Tethyan rifting in Western Cimmeria. *Lithos*, 162-163: 264-278.
- Shervais, J.W., 1982. Ti-V plots and the petrogenesis of modern and ophiolitic lavas. *Earth and Planetary Science Letters*, 57: 101-118.
- Sun, S.S., 1980. Lead isotopic study of young volcanic rocks from mid-ocean ridges, Ocean Island and island arcs. *Philosophical Transactions of the Royal Society of London*, A297: 409-45.
- Sun, S.S., McDonough, W.F., 1989. Chemical and isotopic systematics of oceanic basalts: implications for mantle composition and processes. In: Saunders AD, Norry MJ (eds) *Magmatism in the Ocean Basins*. Geological Society London Special Publication, 42: 313–45.
- Vallance, T.S., 1974. Pyroxenes and the basalt-spilite relation. In: Amstutz, G.C. (Eds), *Spilites and Spilitic Rocks*. International Union of Geological Sciences, Springer, Heidelberg. Pp 59–68.
- Westaway, R., 1994. Present-day kinematics of the Middle East and Eastern Mediterranean. *Journal of Geophysical Research*, 99: 12071-12090.
- Winchester, J.A., Floyd, P.A., 1977. Geochemical discrimination of different magma series and their differentiation products using immobile elements. *Chemical Geology*, 20: 325-343.